

FAST ESTIMATION OF FREQUENCY AND 2-D DOAS FOR CYLINDRICAL CONFORMAL ARRAY ANTENNA USING STATE-SPACE AND PROPAGATOR METHOD

Weijian Si¹, Liangtian Wan^{1, *}, Lutao Liu¹, and Zuoxi Tian²

¹College of Information & Communication Engineering, Harbin Engineering University, Harbin 150001, China

²Science and Technology on Underwater Test and Control Laboratory, Dalian 116013, China

Abstract—The pattern of each element in conformal array has a different direction for the curvature of conformal carrier, which results in polarization diversity of conformal array antenna. Polarization parameters of incident signals are considered in snapshot data model in order to describe the polarization diversity of conformal array antenna. It is required that the polarization parameters and direction of arrival (DOA) of incident signals are estimated together. An integrated frequency and DOA estimation method is proposed in this paper for cylindrical conformal array antenna. The frequency estimation of signal source is obtained by constructing state-space matrix. Through well-designed configuration of elements on cylindrical carriers along with estimation of signal parameters via propagator method (PM), the decoupling scheme for DOA and polarization parameters is implemented. A novel parameter pairing method for frequency and DOA of multiple sources utilizing the interpolation technique is given, based on which the fast frequency-DOA estimation algorithm is developed. Effectiveness of the proposed method is demonstrated by simulation experimental results.

1. INTRODUCTION

Conformal antenna array, i.e., array antennas with antenna elements arranged conformal on a curved surface, will find its potential and promising applications in a variety of fields ranging from space-borne, airborne, ship-borne, and missile-borne radar, space vehicles,

Received 11 December 2012, Accepted 4 February 2013, Scheduled 10 February 2013

* Corresponding author: Liangtian Wan (wanliangtian1@163.com).

wireless communication to sonar [1, 2]. Its advantages include dramatic reduction of aerodynamic drag and the weight of arrays, wide angle coverage of 360° , space-saving, reduction of radar cross-section, as well as potential increase in available aperture. Much of the existing research in conformal antenna array has mainly focused on the design of antenna elements [3–5], the pattern synthesis and optimization of conformal antenna [6–10]. The high resolution direction of arrival (DOA) estimation algorithms [11–14] based on conformal antenna array has not been studied as intensively [15, 16].

Most high resolution DOA estimation algorithms, such as multiple signal classification (MUSIC)-based and estimation of signal parameters via rotational invariance techniques (ESPRIT)-based algorithms, when used on uniform linear array with omni-direction antenna elements, always have high performances [17–19]. But usually, these algorithms cannot be used for conformal antenna array directly because of the varying curvature. Therefore, conformal antenna array presents many challenges to the high resolution DOA estimation. Firstly, MUSIC algorithm estimates DOA of incident signals for every array geometry. If the steering vector of the array is incomplete (Conformal array has the “shadow effect” due to the metallic cylinder, meaning that only the incident wave from a special angle, rather than all the antenna elements can receive this signal), the performance of MUSIC algorithm deteriorates quickly [15]. Sub-array divided MUSIC algorithm could solve this problem efficiently. However, the complexity of the spectral searching may still be too high. The interpolated ESPRIT algorithm has been applied to the conformal antenna array in order to reduce the calculation complexity; nevertheless, the performance is still affected by the interpolated error [16]. Secondly, the element pattern is always defined in the element local coordinates, which leads to a polarization diversity characteristic of the conformal antenna array. In order to describe the polarization diversity characteristic, the polarization parameters of incident signals are considered in the snapshot data model of the conformal antenna array [20]. Thirdly, the mutual coupling between elements becomes more complicated and thus has to be taken into account. These characters restrict the application of conventional DOA algorithms on conformal antenna array for direction finding. The proposed algorithms in [14] could be used when the incident signals have the same frequency, but it could not be used when the incident signals have different frequencies. With the help of state-space and ESPRIT algorithm, the 2-D parameters estimation of joint frequency and angle has been turned into two 1-D parameters estimation [21]. However, polarization diversity characteristic makes it difficult to use

these ESPRIT algorithms on conformal antenna array.

In this paper, state-space and PM algorithm proposed in [23] are integrated to achieve the fast frequency and 2-D angle estimation based on the mathematics model of conformal antenna array proposed in [20]. And a novel parameters pairing method of frequency and DOA using the interpolation technique is proposed. Simulation results indicate the efficiency and accurately of the proposed algorithm. The remainder of this paper is organized as follows. In Section 2, the design configuration of elements on cylindrical carriers and the signal model of arbitrary conformal array configurations with polarization diversity are introduced. In Section 3, state-space and PM algorithm based on divided sub-array technique is described in detail. The parameters pairing methods are discussed. In Section 4, the Cramer-Rao Bound (CRB) is derived. Section 5 provides some final conclusions.

2. THE ELEMENTS CONFIGURATION ON CYLINDRICAL CARRIERS AND THE NARROWBAND DATA MODEL

2.1. The Elements Configuration on Cylindrical Carriers

Unlike ordinary circular array, conformal array has a “shadow effect” due to the metallic cylinder, which means that only the incident wave from a special angle, rather than all of the antenna elements can receive this signal. The sub-array divided technique proposed in [16] is adopted in this paper. Three sub-arrays are divided averagely, and each sub-array is in charge of azimuth coverage of 120° . According to the summery in the cylindrical structure, each sub-array has the same structure. Therefore, the parameters estimation method of each sub-array is exactly the same. All the analysis and simulation depend on

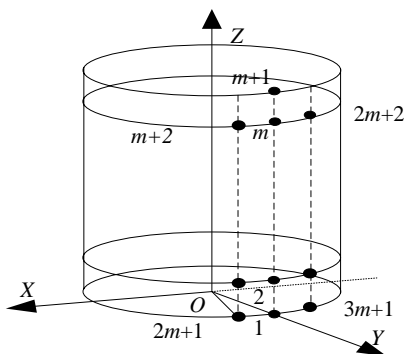


Figure 1. The sub-array structure of cylindrical conformal antenna array.

sub-array 1 in this paper. The parameters estimation results of three sub-arrays are synthesized in order to estimate the incident signals' parameters for the scope of the entire space. Fig. 1 represents the model of cylindrical conformal array, and the elements configuration is well arranged on cylindrical carriers. The distance of the adjacent element in the same cross section is $\lambda/4$, the distance of the adjacent cross section is $\lambda/4$, and the radius of the cylindrical cross section is 5λ , λ represents the shortest wavenumber of the incident signals.

2.2. The Narrowband Data Model of Conformal Array

Assuming that the sampling frequency of the system is $f_s = 1/T_s$, T_s represents the sampling intervals ($T_s < 1/2f_{\max}$, and f_{\max} denotes the highest frequency of incident signals). According to the incident signal based on the assumption of the narrowband and far field, the normalized incident signal has the equation $s_i(n+1) = \phi_i s_i(n)$, where i ($i = 1, 2, \dots, r$) is the i th incident signal, r is source number, and $s(n)$ is the discrete sampling sequence of the incident signal. $\phi_i = \exp(-j2\pi f_i/f_s)$ is the time-shift factor, and f_i denotes the frequency of the i th incident signal. In Fig. 2, the model of incident signal is constructed, and \mathbf{u} is the direction vector of the incident signal with elevation θ and azimuth φ .

Establishing the model of array to receive data accurately is a prerequisite to parameter estimation. The steering vector captures the essence of array antenna's response to a unit intensity of the incident signal space. For conformal array antenna, the element pattern in different location has different direction because of the varying curvature. In the process of constructing the model for conformal antenna, the impact of each element pattern must be taken into account. In this paper we combine the models constructed in [15, 20]. The steering vector of the conformal array antenna is given by

$$\mathbf{a}(\theta, \varphi, f) = \left[r_1 e^{-j2\pi c \frac{\mathbf{P}_1 \cdot \mathbf{u}}{f}}, r_2 e^{-j2\pi c \frac{\mathbf{P}_2 \cdot \mathbf{u}}{f}}, \dots, r_M e^{-j2\pi c \frac{\mathbf{P}_M \cdot \mathbf{u}}{f}} \right]^T \quad (1)$$

$$r_i = (g_{i\theta}^2 + g_{i\varphi}^2)^{1/2} (k_\theta^2 + k_\varphi^2)^{1/2} \cos(\theta_{igk}) \\ = |g_i| |p_l| \cos(\theta_{igk}) = \mathbf{g}_i \cdot \mathbf{p}_l = g_{i\theta} k_\theta + g_{i\varphi} k_\varphi \quad (2)$$

$$\mathbf{P}_i = \sin(\theta_{oi}) \cos(\varphi_{oi}) \mathbf{x} + \sin(\theta_{oi}) \sin(\varphi_{oi}) \mathbf{y} + \cos(\theta_{oi}) \mathbf{z} \quad (3)$$

$$\mathbf{u} = \sin(\theta) \cos(\varphi) \mathbf{x} + \sin(\theta) \sin(\varphi) \mathbf{y} + \cos(\theta) \mathbf{z} \quad (4)$$

$$\mathbf{g}_i = g_{i\theta}(\theta, \varphi) \mathbf{u}_\theta + g_{i\varphi}(\theta, \varphi) \mathbf{u}_\varphi \quad (5)$$

$$\mathbf{u}_\theta = \sin(\theta) \cos(\varphi) \mathbf{x} + \sin(\theta) \sin(\varphi) \mathbf{y} + \cos(\theta) \mathbf{z} \quad (6)$$

$$\mathbf{u}_\varphi = -\sin(\varphi) \mathbf{x} + \cos(\varphi) \mathbf{y} \quad (7)$$

where \mathbf{P}_i is the position vector of the i th element which is in the global

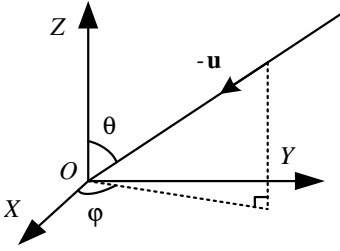


Figure 2. The direction vector \mathbf{u} of the incident signal.

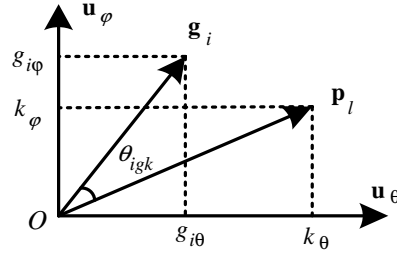


Figure 3. The element's response to the incident signal.

coordinate. θ_{oi} and φ_{oi} are the elevation and azimuth respectively for direction vector of the i th element in the global coordinate. \mathbf{u} is the direction vector of the narrowband far field incident signal with elevation θ and azimuth φ in the global coordinate. f and c represent the frequency and light velocity respectively. As shown in Fig. 3, k_θ and k_φ are the component products which projected the incident signal polarization vector onto polarization basis vectors \mathbf{u}_θ and \mathbf{u}_φ respectively. \mathbf{u}_θ and \mathbf{u}_φ are orthogonal unit vector. \mathbf{g}_i is a unit pattern. \mathbf{p}_l is direction vector of electric field. r_i is the element's response to the i th unit strength incident signal in the global coordinate. $g_{i\theta}$, $g_{i\varphi}$ are the component products which projected the i th element pattern onto \mathbf{u}_θ and \mathbf{u}_φ respectively. θ_{igk} is the angle between the vector \mathbf{g}_i and \mathbf{p}_l , and $(\cdot)^T$ denotes the transpose.

The narrowband snapshot data model of conformal array antenna is expressed as

$$\begin{aligned} \mathbf{X}(n) &= \mathbf{G} \cdot \mathbf{A} \mathbf{S}(n) + \mathbf{N}(n) \\ &= (\mathbf{G}_\theta \cdot \mathbf{A}_\theta \mathbf{K}_\theta + \mathbf{G}_\varphi \cdot \mathbf{A}_\varphi \mathbf{K}_\varphi) \mathbf{S}(n) + \mathbf{N}(n) = \mathbf{B} \mathbf{S}(n) + \mathbf{N}(n) \end{aligned} \quad (8)$$

$$\mathbf{S}(n) = [s_1(n), s_2(n), \dots, s_r(n)]^T \quad (9)$$

$$\mathbf{N}(n) = [n_1(n), n_2(n), \dots, n_r(n)]^T \quad (10)$$

$$\mathbf{G}_\theta = [\mathbf{g}_\theta(\theta_1, \varphi_1, f_1), \mathbf{g}_\theta(\theta_2, \varphi_2, f_2), \dots, \mathbf{g}_\theta(\theta_r, \varphi_r, f_r)] \quad (11)$$

$$\mathbf{G}_\varphi = [\mathbf{g}_\varphi(\theta_1, \varphi_1, f_1), \mathbf{g}_\varphi(\theta_2, \varphi_2, f_2), \dots, \mathbf{g}_\varphi(\theta_r, \varphi_r, f_r)] \quad (12)$$

$$\mathbf{A}_\theta = [\mathbf{a}_\theta(\theta_1, \varphi_1, f_1), \mathbf{a}_\theta(\theta_2, \varphi_2, f_2), \dots, \mathbf{a}_\theta(\theta_r, \varphi_r, f_r)] \quad (13)$$

$$\mathbf{A}_\varphi = [\mathbf{a}_\varphi(\theta_1, \varphi_1, f_1), \mathbf{a}_\varphi(\theta_2, \varphi_2, f_2), \dots, \mathbf{a}_\varphi(\theta_r, \varphi_r, f_r)] \quad (14)$$

$$\mathbf{K}_\theta = \text{diag}(k_{1\theta}, k_{2\theta}, \dots, k_{r\theta}) \quad (15)$$

$$\mathbf{K}_\varphi = \text{diag}(k_{1\varphi}, k_{2\varphi}, \dots, k_{r\varphi}) \quad (16)$$

where \mathbf{G} is the $M \times r$ pattern matrix, and \mathbf{A} is the $M \times r$ manifold matrix. $\mathbf{B} = \mathbf{G} \cdot \mathbf{A}$ includes the incident signal information of DOA and

polarization status. $\mathbf{S}(n)$ is the $r \times 1$ signal vector. $\mathbf{S}(n+1) = \Phi \cdot \mathbf{S}(n)$, $\Phi = \text{diag}[\phi_1, \phi_2, \dots, \phi_r]$ is the time-shift rotational invariance matrix which is used to obtain the frequencies of incident signals. $\mathbf{N}(n)$ is the $M \times 1$ additive Gaussian white noise. $\mathbf{K} = \text{diag}(k_1, k_2, \dots, k_r)$ means that \mathbf{K} is a diagonal matrix, and the main diagonal elements are k_1, k_2, \dots, k_r . θ_i and φ_i represent elevation and azimuth in the global coordinate which respond to the i th incident signal. $k_{i\theta}$ and $k_{i\varphi}$ are the component products which projected the i th incident signal polarization vectors onto \mathbf{u}_θ and \mathbf{u}_φ respectively.

The snapshot data model of conformal array antenna must take into account the fact that the definition and design of each element refer to its local coordinate. A spatial rotation transformation is always necessary to find the element pattern in the array global coordinate. The data received by array is determined by the DOA and polarization parameters of the incident signal. While estimating the DOA of the cylindrical conformal array antenna, the decoupling between the DOA and the polarization must be completed. The pairing of frequency and DOA has also been a challenging problem caused by different element patterns.

3. JOINT FREQUENCY AND ANGLE ESTIMATION

3.1. The Array Structure and the Model of the Receive Data

The array geometry structure used in the proposed algorithm is shown in Fig. 1. $1 \sim m$ is array 1, $2 \sim m+1$ is array 2, $m+2 \sim 2m+1$ is array 3, and $2m+2 \sim 3m+1$ is array 4. The first pair of sub-array 1 consists of array 1 and array 2, the distance vector is $\Delta \mathbf{P}_1$, and $|\Delta \mathbf{P}_1| = \mathbf{d}_1 = \lambda/4$ is shown in Fig. 4(a). From Fig. 4(b), it can be seen that the second pair of sub-array 2 consists of array 1 and array 3, the distance vector is $\Delta \mathbf{P}_2$. The third pair of sub-array 3 consists of array 1 and array 4, the distance vector is $\Delta \mathbf{P}_3$, $|\Delta \mathbf{P}_2| = \mathbf{d}_2 = |\Delta \mathbf{P}_3| = \mathbf{d}_3 = \lambda/4$. The elements which share the same busbar have the same pattern direction, therefore the elements from 1 to $m+1$ have the same pattern \mathbf{g}_1 , the elements from $m+2$ to $2m+1$ have the same pattern \mathbf{g}_2 , and the elements from $2m+2$ to $3m+1$ have the same pattern \mathbf{g}_3 . If we make full use of the characteristics of the array structure, the coupling between the DOA and the polarization could be solved.

Assuming that $\mathbf{X}_1, \mathbf{X}_2, \mathbf{X}_3, \mathbf{X}_4$ stand for array 1, array 2, array 3, array 4 respectively, and the coordinate origin is regarded as a reference point of the received signals. The signal that each array receives can be represented as

$$\mathbf{X}_1 = \mathbf{B}\mathbf{S} + \mathbf{N}_1 \quad (17)$$

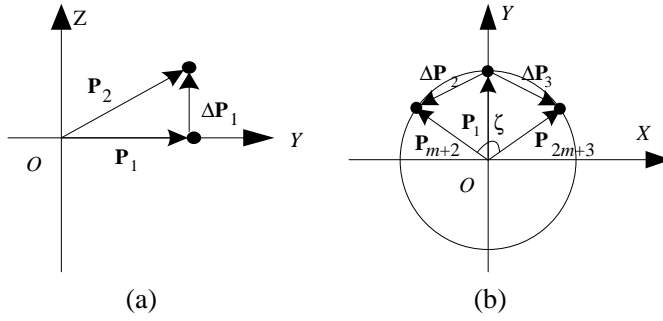


Figure 4. (a) The distance vector $\Delta\mathbf{P}_1$ between array 1 and array 2. (b) The distance vector $\Delta\mathbf{P}_2$ between array 1 and array 3, and the distance vector $\Delta\mathbf{P}_3$ between array 1 and array 4.

$$\mathbf{X}_2 = \mathbf{B}\Psi_1\mathbf{S} + \mathbf{N}_2 \tag{18}$$

$$\mathbf{X}_3 = \mathbf{B}\Psi_2\mathbf{S} + \mathbf{N}_3 \tag{19}$$

$$\mathbf{X}_4 = \mathbf{B}\Psi_3\mathbf{S} + \mathbf{N}_4 \tag{20}$$

where

$$\Psi_1 = \text{diag} [\exp(-j\omega_{11}), \exp(-j\omega_{12}), \dots, \exp(-j\omega_{1r})] \tag{21}$$

$$\Psi_2 = \text{diag} \left[\frac{r_3(\theta_1, \varphi_1, f_1)}{r_1(\theta_1, \varphi_1, f_1)} \exp(-j\omega_{21}), \right. \\ \left. \frac{r_3(\theta_2, \varphi_2, f_2)}{r_1(\theta_2, \varphi_2, f_2)} \exp(-j\omega_{22}), \dots, \frac{r_3(\theta_r, \varphi_r, f_r)}{r_1(\theta_r, \varphi_r, f_r)} \exp(-j\omega_{2r}) \right] \tag{22}$$

$$\Psi_3 = \text{diag} \left[\frac{r_4(\theta_1, \varphi_1, f_1)}{r_1(\theta_1, \varphi_1, f_1)} \exp(-j\omega_{31}), \right. \\ \left. \frac{r_4(\theta_2, \varphi_2, f_2)}{r_1(\theta_2, \varphi_2, f_2)} \exp(-j\omega_{32}), \dots, \frac{r_4(\theta_r, \varphi_r, f_r)}{r_1(\theta_r, \varphi_r, f_r)} \exp(-j\omega_{3r}) \right] \tag{23}$$

$$\omega_{1i} = (2\pi f_i/c) d_1 \Delta\mathbf{P}_1 \cdot \mathbf{u}_i \\ = (2\pi d_1 f_i/c) [\sin(\theta_{\Delta\mathbf{P}_1}) \cos(\varphi_{\Delta\mathbf{P}_1}) \sin(\theta_i) \cos(\varphi_i) \\ + \sin(\theta_{\Delta\mathbf{P}_1}) \sin(\varphi_{\Delta\mathbf{P}_1}) \sin(\theta_i) \sin(\varphi_i) + \cos(\theta_{\Delta\mathbf{P}_1}) \cos(\theta_i)] \tag{24}$$

$$\omega_{2i} = (2\pi f_i/c) d_2 \Delta\mathbf{P}_2 \cdot \mathbf{u}_i \\ = (2\pi d_2 f_i/c) [\sin(\theta_{\Delta\mathbf{P}_2}) \cos(\varphi_{\Delta\mathbf{P}_2}) \sin(\theta_i) \cos(\varphi_i) \\ + \sin(\theta_{\Delta\mathbf{P}_2}) \sin(\varphi_{\Delta\mathbf{P}_2}) \sin(\theta_i) \sin(\varphi_i) + \cos(\theta_{\Delta\mathbf{P}_2}) \cos(\theta_i)] \tag{25}$$

$$\omega_{3i} = (2\pi f_i/c) d_3 \Delta\mathbf{P}_3 \cdot \mathbf{u}_i \\ = (2\pi d_3 f_i/c) [\sin(\theta_{\Delta\mathbf{P}_3}) \cos(\varphi_{\Delta\mathbf{P}_3}) \sin(\theta_i) \cos(\varphi_i) \\ + \sin(\theta_{\Delta\mathbf{P}_3}) \sin(\varphi_{\Delta\mathbf{P}_3}) \sin(\theta_i) \sin(\varphi_i) + \cos(\theta_{\Delta\mathbf{P}_3}) \cos(\theta_i)] \tag{26}$$

$\theta_{\Delta\mathbf{P}_i}$ and $\varphi_{\Delta\mathbf{P}_i}$ represent elevation and azimuth in the global coordinate which respond to the distance vector $\Delta\mathbf{P}_i$. r_i ($i = 1, 2,$

3) is the pattern of each array element. The received data matrix can be reconstructed as:

$$\mathbf{X}_{4m \times r} = [\mathbf{X}_1^T \quad \mathbf{X}_2^T \quad \mathbf{X}_3^T \quad \mathbf{X}_4^T]^T \quad (27)$$

3.2. The Frequency Estimation Based on State-space

In the observation time window, $L+1$ points are sampled. From $\mathbf{S}(n+1) = \mathbf{\Phi} \cdot \mathbf{S}(n)$, we obtain

$$\begin{aligned} \mathbf{X}(k) &= \mathbf{B}\mathbf{S}(k) + \mathbf{N}(k) \\ &= \mathbf{B}\mathbf{\Phi}\mathbf{S}(k-1) + \mathbf{N}(k) = \dots, \dots \mathbf{B}\mathbf{\Phi}^k\mathbf{S}(k) + \mathbf{N}(k) \end{aligned} \quad (28)$$

$4Nm \times (L - N + 1)$ matrix is constructed as:

$$\mathbf{X}_N = \begin{bmatrix} \mathbf{X}(1) & \mathbf{X}(2) & \dots & \mathbf{X}(L-N+1) \\ \mathbf{X}(2) & \mathbf{X}(3) & \dots & \mathbf{X}(L-N+2) \\ \vdots & \vdots & \ddots & \vdots \\ \mathbf{X}(N) & \mathbf{X}(N+1) & \dots & \mathbf{X}(L+1) \end{bmatrix} \quad (29)$$

where N is the temporal smoothing parameter. The temporal smoothing matrix \mathbf{X}_N can be constructed by delaying the row $[\mathbf{X}(1), \mathbf{X}(2), \dots, \mathbf{X}(L-N+1)]$. Assuming that all the incident signals have different frequencies (here, $m > r$). The signals are divided into r groups (each group has the same DOA). Suppose p_i is the number of signal source in the i th group. \mathbf{X}_N is full rank if and only if $N \geq \max_i p_i$. The temporal smoothing approach can distinguish the signals which have the same DOA but different frequencies, more details can be found in [19].

When $N \ll f_s$, we take (28) into (29), then (29) is written in another form

$$\begin{aligned} \mathbf{X}_N &= \begin{bmatrix} \mathbf{B}\mathbf{\Phi}\mathbf{S}(1) & \mathbf{B}\mathbf{\Phi}\mathbf{S}(2) & \dots & \mathbf{B}\mathbf{\Phi}\mathbf{S}(L-N+1) \\ \mathbf{B}\mathbf{\Phi}\mathbf{S}(2) & \mathbf{B}\mathbf{\Phi}^2\mathbf{S}(3) & \dots & \mathbf{B}\mathbf{\Phi}^2\mathbf{S}(L-N+2) \\ \vdots & \vdots & \ddots & \vdots \\ \mathbf{B}\mathbf{\Phi}^N\mathbf{S}(N) & \mathbf{B}\mathbf{\Phi}^N\mathbf{S}(N+1) & \dots & \mathbf{B}\mathbf{\Phi}^N\mathbf{S}(L+1) \end{bmatrix} + \mathbf{N}_N \\ &= \begin{bmatrix} \mathbf{B}\mathbf{\Phi} \\ \mathbf{B}\mathbf{\Phi}^2 \\ \vdots \\ \mathbf{B}\mathbf{\Phi}^N \end{bmatrix} [\mathbf{\Phi}\mathbf{s}(1) \quad \mathbf{\Phi}^2\mathbf{s}(2) \quad \dots \quad \mathbf{\Phi}^N\mathbf{s}(L-N+1)] + \mathbf{N}_N \\ &= (\mathbf{B} \otimes \mathbf{K}) (\mathbf{K}^T \odot \mathbf{s}) + \mathbf{N}_N = \mathbf{B}_N \mathbf{K}_s + \mathbf{N}_N \end{aligned} \quad (30)$$

where \mathbf{K} denotes $[\mathbf{\Phi} \quad \mathbf{\Phi}^2 \quad \dots \quad \mathbf{\Phi}^N]^T$, and \mathbf{s} denotes $[s_1, s_2, \dots, s_r]^T$. \otimes is the left Kronecker product and \odot the Hadamard product. It can be

seen that (30) and (8) have a similar expression form. \mathbf{B} is merely replaced by \mathbf{B}_N . The eigenvalue decomposition of the covariance matrix of \mathbf{X}_N is represented as

$$\mathbf{R} = \sum_{k=1}^{4Nm} \sigma_k^2 \mathbf{u}_k \mathbf{u}_k^H \quad (31)$$

The r eigenvectors are response to the r larger eigenvalues. $\mathbf{u}_1 \mathbf{u}_2, \dots, \mathbf{u}_r$ and \mathbf{B}_N span the same space

$$\text{span}([\mathbf{u}_1 \ \mathbf{u}_2 \ \dots, \ \mathbf{u}_r]) \simeq \text{span}(\mathbf{B}_N) \quad (32)$$

The estimation of signal subspace $\hat{\mathbf{U}}$ is

$$\hat{\mathbf{U}} = [\mathbf{u}_1 \ \mathbf{u}_2 \ \dots, \ \mathbf{u}_r] \quad (33)$$

There exists a unknown $r \times r$ matrix \mathbf{T} , then the transform matrices \mathbf{B}_T and Φ_T are represented as

$$\begin{aligned} \hat{\mathbf{B}}_T &= \hat{\mathbf{B}}\mathbf{T} = (\hat{\mathbf{U}})_{1:1} \\ \hat{\Phi}_T &= \mathbf{T}^{-1}\Phi\mathbf{T} = (\hat{\mathbf{U}})_{1:4m-1}^\dagger (\hat{\mathbf{U}})_{2:4m} \end{aligned} \quad (34)$$

where $(\cdot)^\dagger$ denotes the Moore-Penrose pseudoinverse, and $(\hat{\mathbf{U}})_{k:l}$ is the sub-array from the k th to the l th (the sub-array is $4m \times r$). $\hat{\Phi}_T$ and Φ have the same eigenvalues. The eigenvalue decomposition of Φ_T can be represented as

$$\Phi_T = \mathbf{E}\Lambda\mathbf{E}^{-1} \quad (35)$$

It is known that the eigenvalues of Φ_T correspond to the eigenvalues of Φ , therefore, the estimation of frequencies for the incident signals can be obtained as

$$f_i = [\text{angle}(\phi_i) \times f_s] / 2\pi, \quad i = 1, 2, \dots, r \quad (36)$$

A diagonalization of Φ_T is completed by \mathbf{E} , which provides a estimation of transform matrix \mathbf{T}^{-1}

$$\hat{\mathbf{B}} = \hat{\mathbf{B}}_T\mathbf{E} \quad (37)$$

3.3. The DOA Estimation Based on PM Algorithm

Since the steering vector has column full rank and r rows of \mathbf{B} are linearly independent, other rows can be represented by these r rows. Assuming that the former r rows are linearly independent, the steering vector \mathbf{B} is divided into 2 blocks

$$\mathbf{B} = [\mathbf{B}_1^T \ \mathbf{B}_2^T]^T \quad (38)$$

\mathbf{B}_1 and \mathbf{B}_2 are $r \times r$ and $(m - r) \times r$ matrices.

The propagator \mathbf{V} is defined as

$$\mathbf{V}^H \mathbf{B}_1 = \mathbf{B}_2 \quad (39)$$

The $4m \times r$ matrix can be constructed as

$$\mathbf{C}_{4m \times r} = [\mathbf{B}^T \quad (\mathbf{B}\Psi_1)^T \quad (\mathbf{B}\Psi_2)^T \quad (\mathbf{B}\Psi_3)^T]^T \quad (40)$$

The matrix \mathbf{C} is also divided into 2 blocks

$$\mathbf{C} = [\mathbf{B}_1^T \quad \mathbf{C}_1^T]^T \quad (41)$$

where

$$\mathbf{C}_1 = [\mathbf{B}_2^T (\mathbf{B}_1\Psi_1)^T \quad (\mathbf{B}_2\Psi_1)^T \quad (\mathbf{B}_1\Psi_2)^T \quad (\mathbf{B}_2\Psi_2)^T \quad (\mathbf{B}_1\Psi_3)^T \quad (\mathbf{B}_2\Psi_3)^T] \quad (42)$$

$\mathbf{C}_1 = \bar{\mathbf{V}}^H \mathbf{B}_1$, and $\bar{\mathbf{V}}$ is the propagator whose dimension is $r \times [4m - r]$.

From (37), the matrix $\hat{\mathbf{B}}$ is divided into 2 blocks

$$\hat{\mathbf{B}} = [\hat{\mathbf{B}}_1^T \quad \hat{\mathbf{B}}_2^T] \quad (43)$$

where, $\hat{\mathbf{B}}_1$ is $r \times r$ matrix, and $\hat{\mathbf{B}}_2$ is $(4m - r) \times r$ matrix. The propagator $\bar{\mathbf{V}}$ can be represented as

$$\bar{\mathbf{V}} = \left(\hat{\mathbf{B}}_2 \hat{\mathbf{B}}_1^{-1} \right)^H \quad (44)$$

The matrix $\hat{\mathbf{B}}$ is divided into 7 blocks, which are equal to the 7 blocks of the matrix \mathbf{C}_1 respectively. When $r \leq [4m - r]$, i.e., $r \leq 2m$, the right inverse matrix $\bar{\mathbf{V}}^\#$ of $\bar{\mathbf{V}}$ is

$$\bar{\mathbf{V}}^\# = (\bar{\mathbf{V}}^H \bar{\mathbf{V}})^{-1} \bar{\mathbf{V}}^H \quad (45)$$

The equation is obtained by combining (42) and (45)

$$\bar{\mathbf{V}}_1^\# \bar{\mathbf{V}}_3 \mathbf{B}_1 = \mathbf{B}_1 \Psi_1 \quad (46)$$

$$\bar{\mathbf{V}}_1^\# \bar{\mathbf{V}}_5 \mathbf{B}_1 = \mathbf{B}_1 \Psi_2 \quad (47)$$

$$\bar{\mathbf{V}}_1^\# \bar{\mathbf{V}}_7 \mathbf{B}_1 = \mathbf{B}_1 \Psi_3 \quad (48)$$

It can be seen that the eigenvalues $[\lambda_{11} \lambda_{12} \dots \lambda_{1r}]$, $[\lambda_{21} \lambda_{22} \dots \lambda_{2r}]$, $[\lambda_{31} \lambda_{32} \dots \lambda_{3r}]$ of $\bar{\mathbf{V}}_1^\# \bar{\mathbf{V}}_3$, $\bar{\mathbf{V}}_1^\# \bar{\mathbf{V}}_5$, $\bar{\mathbf{V}}_1^\# \bar{\mathbf{V}}_7$ are corresponding to the diagonal elements of Ψ_1 , Ψ_2 , Ψ_3 . The DOA estimation of signals is acquired under the condition that the frequencies of incident signals are already known.

Because r_1 , r_3 and r_4 are real numbers, the phase ambiguous problem caused by the positive and negative inconsistent of r_1 , r_3 and

r_4 , is solved by eigenvalues λ_{2i} and λ_{3i} squared.

$$\omega_{1i} = -\text{angle}(\lambda_{1i}) \tag{49}$$

$$\begin{aligned} \omega_{2i} &= -\frac{1}{2} \text{angle} \left(\left[\frac{r_3(\theta_i, \varphi_i, f_i)}{r_1(\theta_i, \varphi_i, f_i)} \exp(-j\omega_{2i}) \right]^2 \right) \\ &= -\frac{1}{2} \text{angle} \left(\exp(-j\omega_{2i})^2 \right) = -\frac{1}{2} \text{angle} \left((\lambda_{2i})^2 \right) \end{aligned} \tag{50}$$

$$\omega_{3i} = -\frac{1}{2} \text{angle} \left((\lambda_{3i})^2 \right) \tag{51}$$

Assuming that $\Delta p_{12} = \sin(\theta_{\Delta \mathbf{P}_1}) \sin(\varphi_{\Delta \mathbf{P}_1})$, $\Delta p_{13} = \cos(\theta_{\Delta \mathbf{P}_1})$, $\Delta p_{2i}, \Delta p_{3i}$ ($i = 1, 2, 3$); $\gamma_{1i} = \sin(\theta_i) \cos(\varphi_i)$, $\gamma_{2i} = \sin(\theta_i) \sin(\varphi_i)$, $\gamma_{3i} = \cos(\theta_i)$. The equation is determined by solving (24), (25), (26) and (49), (50), (51) simultaneously

$$-\frac{c}{2\pi} \begin{bmatrix} \frac{\text{angle}(\lambda_{1i})}{\mathbf{d}_1 f_i} \\ \frac{\text{angle}((\lambda_{2i})^2)}{2\mathbf{d}_2 f_i} \\ \frac{\text{angle}((\lambda_{3i})^2)}{2\mathbf{d}_3 f_i} \end{bmatrix} = \begin{bmatrix} \Delta p_{11} & \Delta p_{11} & \Delta p_{11} \\ \Delta p_{11} & \Delta p_{11} & \Delta p_{11} \\ \Delta p_{11} & \Delta p_{11} & \Delta p_{11} \end{bmatrix} \begin{bmatrix} \gamma_{1i} \\ \gamma_{2i} \\ \gamma_{3i} \end{bmatrix} \tag{52}$$

The solution of (52) is

$$\begin{bmatrix} \gamma_{1i} \\ \gamma_{2i} \\ \gamma_{3i} \end{bmatrix} = -\frac{c}{2\pi} \begin{bmatrix} \Delta p_{11} & \Delta p_{11} & \Delta p_{11} \\ \Delta p_{11} & \Delta p_{11} & \Delta p_{11} \\ \Delta p_{11} & \Delta p_{11} & \Delta p_{11} \end{bmatrix}^{-1} \begin{bmatrix} \frac{\text{angle}(\lambda_{1i})}{\mathbf{d}_1 f_i} \\ \frac{\text{angle}((\lambda_{2i})^2)}{2\mathbf{d}_2 f_i} \\ \frac{\text{angle}((\lambda_{3i})^2)}{2\mathbf{d}_3 f_i} \end{bmatrix} \tag{53}$$

There are two ways to solve the angle θ_i and φ_i .

One way is

$$\begin{aligned} \theta_i &= \arccos \gamma_{3i} \\ \varphi_i &= \arcsin \left(\frac{\gamma_{1i}}{\cos(\theta_i)} \right) \quad \text{or} \quad \varphi_i = \arcsin \left(\frac{\gamma_{2i}}{\sin(\theta_i)} \right) \end{aligned} \tag{54}$$

The other way is

$$\begin{aligned} \varphi_i &= \arctan \left(\frac{\gamma_{2i}}{\gamma_{1i}} \right) \\ \theta_i &= \arccos \left(\frac{\gamma_{1i}}{\cos(\varphi_i)} \right) \quad \text{or} \quad \theta_i = \arcsin \left(\frac{\gamma_{2i}}{\sin(\varphi_i)} \right) \end{aligned} \tag{55}$$

The joint frequency and angle estimation for the cylindrical conformal array antenna are completed. However, under the condition that the signal source number $r \geq 2$, the eigenvalues of the 2D-DOA cannot be paired accurately, and the frequency and angle cannot be paired appropriately either due to the varying curvature.

3.4. The Pairing Method

In practical calculations the eigenvalue decomposition of Ψ_1, Ψ_2, Ψ_3 is done independently. As a result, the sequence of eigenvector may be different from each other. The sequence of eigenvector should be adjusted in order to obtain the accurate parameters. In this paper, the eigenvalue and eigenvector matrices $\mathbf{T}_1, \mathbf{T}_2, \mathbf{T}_3$ are obtained through eigenvalue decomposition of Ψ_1, Ψ_2, Ψ_3 . Since the eigenvectors corresponding to the eigenvalues of $\mathbf{T}_1, \mathbf{T}_2, \mathbf{T}_3$ are not relevant to each other, let $\mathbf{G}_1 = \mathbf{T}_1^H \mathbf{T}_2$, the largest element value in each row of matrix \mathbf{G}_1 can be utilized to achieve the eigenvalue pairing of Ψ_1, Ψ_2 . The eigenvalue pairing of Ψ_1, Ψ_3 and Ψ_2, Ψ_3 be achieved using the same approach.

Since the conventional parameter pairing methods could not be used under the varying curvature situation, the 2-D interpolation technique is adopted to achieve the pairing of frequency and angle. It is necessary for the 2-D interpolation algorithm to interpolate values at the direction of φ and θ simultaneously. The impact of different frequencies on the interpolation values should be taken into account. In practice, the 3-D interpolation method is used here. Interpolation of frequency value is carried out at first. According to the order of magnitude for the frequency estimation (e.g., kHz, MHz, GHz), the interpolation value is one thousandth of the order of frequency magnitude. In this paper, Assuming that frequency ranges from f_a to f_b (the order of magnitude is GHz), one interpolation value is taken at each MHz intervals. The 2-D interpolation value from f_a to f_b can be represented as

$$\begin{aligned}
 [\Phi_a, \Theta_a] &= [(\varphi, \theta)_{a1}, (\varphi, \theta)_{a2}, \dots, (\varphi, \theta)_{aK}] \\
 &\quad \vdots \quad \quad \quad \vdots \quad \quad \quad \vdots \quad \quad \quad \vdots \\
 [\Phi_j, \Theta_j] &= [(\varphi, \theta)_{j1}, (\varphi, \theta)_{j2}, \dots, (\varphi, \theta)_{jK}] \\
 &\quad \vdots \quad \quad \quad \vdots \quad \quad \quad \vdots \quad \quad \quad \vdots \\
 [\Phi_b, \Theta_b] &= [(\varphi, \theta)_{b1}, (\varphi, \theta)_{b2}, \dots, (\varphi, \theta)_{bK}]
 \end{aligned} \tag{56}$$

where $K = K_1 \times K_2$, K_1 is the number of interpolation values at the direction φ , and K_2 is the number of interpolation values at the direction θ . For instance, at f_a , the real array manifold via interpolation is transformed as

$$\begin{aligned}
 \mathbf{G}_a \cdot \mathbf{A}_a &= [\mathbf{f}(\varphi, \theta)_{a1} \mathbf{a}(\varphi, \theta)_{a1}, \mathbf{f}(\varphi, \theta)_{a2} \mathbf{a}(\varphi, \theta)_{a2}, \dots, \\
 &\quad \mathbf{f}(\varphi, \theta)_{aK} \mathbf{a}(\varphi, \theta)_{aK}] \in \mathbb{C}^{MN \times K}
 \end{aligned} \tag{57}$$

where MN is the total number of virtual array elements. After

interpolation, the manifold for virtual array $\bar{\mathbf{A}}_a$ becomes

$$\bar{\mathbf{A}}_a = [\bar{\mathbf{a}}(\varphi, \theta)_{a1}, \bar{\mathbf{a}}(\varphi, \theta)_{a2}, \dots, \bar{\mathbf{a}}(\varphi, \theta)_{aK}] \in \mathbb{C}^{MN \times K} \quad (58)$$

The transformation matrix \mathbf{B}_a can be found to satisfy (59)

$$\tau = \frac{\|\bar{\mathbf{A}}_a - \mathbf{B}_a^H(\mathbf{G}_a \cdot \mathbf{A}_a)\|_F}{\|\mathbf{G}_a \cdot \mathbf{A}_a\|_F} \quad (59)$$

$\|\cdot\|_F$ denotes the Frobenius norm. If τ is small enough, for example, 0.001, then accept \mathbf{B}_a . The position of elements is known exactly, and the matrix \mathbf{A}_a is determined. Using $\bar{\mathbf{A}}_a = \mathbf{B}_a^H(\mathbf{G}_a \cdot \mathbf{A}_a)$, the pattern matrix \mathbf{G}_a is obtained. The pattern matrix for other frequency point can be obtained in the same way. More details about interpolation technique can be found in [24–26]. Although the virtual transformation is computationally intensive, it could be done off-line as a preprocessing step. The matrix \mathbf{B}_a needs to be computed only once and stored in the system for any given array. We can find the pattern corresponding to the frequency and angle after the frequency and angle are estimated.

The first m rows in $\hat{\mathbf{B}}_1$ are extracted from the matrix $\hat{\mathbf{B}}$. The frequencies and angles are used to construct the matrix $\hat{\mathbf{A}}_1$, the pattern matrix \mathbf{g}_1 is found in the system simultaneously. If the frequency and angle are paired successfully, the Equation (60) should be satisfied

$$\min \left\| \hat{\mathbf{B}}_1 - \mathbf{g}_1 \cdot \hat{\mathbf{A}}_1 \right\|_F, \theta_i, \varphi_i, f_i \quad (i = 1, 2, \dots, r) \quad (60)$$

where $\min \|\cdot\|$ is the minimum of the Frobenius norm.

The algorithm is summarized in the following steps:

- 1) Divide the whole array into 3 sub-arrays using the method illustrated in [15];
- 2) For (31), the estimation matrix \hat{R}_{X_N} of covariance matrix \mathbf{R} is achieved by using the limited length sampling data.
- 3) The eigenvalue decomposition of \hat{R}_{X_N} is done, and the signal subspace $\hat{\mathbf{U}}_s$ corresponding to \hat{R}_{X_N} is obtained.
- 4) According to (36), the frequency estimation \hat{f}_i of the incident signal is obtained.
- 5) According to (44), the propagator $\bar{\mathbf{V}}$ is acquired. The matrix $\bar{\mathbf{V}}$ is divided into 7 blocks from $\bar{\mathbf{V}}_1$ to $\bar{\mathbf{V}}_7$ corresponding to the 7 blocks of \mathbf{C}_1 .
- 6) According to (54) or (55), the DOA estimation is completed estimation of frequencies.
- 7) The pairing of 2-D DOA is done, at first and the pairing of frequency and angle using (60) is completed at last. The integrated joint frequency and angle estimation for cylindrical conformal antenna array is accomplished.

4. CRAMER-RAO LOWER BOUND

Setting a lower bound proves to be extremely useful for any estimator. It provides a benchmark against which we can compare the performance of any unbiased estimator. Moreover, it tells us the impossibility of finding an unbiased estimator whose variance is less than the bound. One such bound is the CRB [27]. We derive the CRB for the algorithm proposed in this paper. The derivation process approximates the method proposed in [22].

Assuming a $P \times 1$ deterministic signal vector $\mathbf{s}(k; \mathbf{u})$ with unknown parameter vector is

$$\mathbf{u} = [\mathbf{u}_1 \quad \mathbf{u}_2 \quad \dots \quad \mathbf{u}_q] \quad (61)$$

The observation vector with additive noise is

$$\mathbf{x}(k) = \mathbf{s}(k; \mathbf{u}) + \mathbf{n}(k) = \begin{bmatrix} \mathbf{s}_1(k; \mathbf{u}) \\ \mathbf{s}_2(k; \mathbf{u}) \\ \dots \\ \mathbf{s}_p(k; \mathbf{u}) \end{bmatrix} + \mathbf{n}(k) \in \mathbb{C}^P \quad (62)$$

where $\mathbf{n}(k)$ is a $P \times 1$ noise vector. Assume that $\mathbf{n}(k)$ is a white Gaussian noise (WGN) with σ^2 variance and we have collected M time samples of the signal $\mathbf{x}(k)$. Then, the log likelihood function of the signal can be written as

$$L(\mathbf{x}; \mathbf{u}) = -\frac{MP}{2} \ln(2\pi\sigma^2) - \frac{1}{2\sigma^2} \sum_{k=1}^M [\mathbf{x}(k) - \mathbf{s}(k; \mathbf{u})]^H [\mathbf{x}(k) - \mathbf{s}(k; \mathbf{u})] \quad (63)$$

The gradient of the signal vector $\mathbf{s}(k; \mathbf{u})$ with respect to \mathbf{u} is denoted by $\mathbf{D}_k(\mathbf{u})$, i.e.,

$$\mathbf{D}_k(\mathbf{u}) = \begin{bmatrix} \frac{\partial \mathbf{s}(k; \mathbf{u})}{\partial u_1} & \frac{\partial \mathbf{s}(k; \mathbf{u})}{\partial u_2} & \dots & \frac{\partial \mathbf{s}(k; \mathbf{u})}{\partial u_q} \end{bmatrix} \quad (64)$$

then the so-called Fisher information matrix is given by

$$\mathbf{I}(\mathbf{u}) = \frac{1}{\sigma^2} \text{Re} \left(\sum_{k=1}^M \mathbf{D}_k^H(\mathbf{u}) \mathbf{D}_k(\mathbf{u}) \right) \quad (65)$$

The CRB for estimating the i th parameter u_i is obtained from the inverse of the Fisher information matrix as

$$\text{CRB}(u_i) = [\mathbf{I}^{-1}(\mathbf{u})]_{ii} \quad (66)$$

In order to simplify the derivation process, the source correlation matrix is assumed to be known. So the covariance matrix \mathbf{R}

contains $5r$ unknown parameters, i.e., r frequency parameters, $2r$ angle parameters, and $2r$ polarization parameters. Since the decoupling between the angle and the polarization has been done, only $3r$ parameters need to be estimated, which can be expressed as a vector

$$\mathbf{p} = [f_1, \theta_1, \varphi_1, f_2, \theta_2, \varphi_2, \dots, f_{3r}, \theta_{3r}, \varphi_{3r}] \quad (67)$$

The model in (28) is simplified as

$$\mathbf{x}(k) = \mathbf{B}(\theta, \varphi) \Phi^k + \mathbf{n}(k) \quad (68)$$

The unknown $3r \times 1$ parameter vector is

$$\mathbf{u} = [\mathbf{f}\theta\varphi]^T \quad (69)$$

Define

$$\mathbf{D}(\theta) = \begin{bmatrix} \frac{\partial \mathbf{b}_1(\theta_1, \varphi_1)}{\partial \theta_1} & \frac{\partial \mathbf{b}_2(\theta_2, \varphi_2)}{\partial \theta_2} & \dots & \frac{\partial \mathbf{b}_r(\theta_r, \varphi_r)}{\partial \theta_r} \end{bmatrix} \quad (70)$$

$$\Phi^k = \text{diag} \{ \varphi^k \}.$$

Evaluating the derivative of $\mathbf{s}(k; \mathbf{u})$ with respect to each parameter, we get the following:

$$\frac{\partial \mathbf{s}(k; \mathbf{u})}{\partial \theta} = \mathbf{D}_\theta \Phi^k =: \mathbf{D}_k(\theta)$$

$$\frac{\partial \mathbf{s}(k; \mathbf{u})}{\partial \varphi} = \mathbf{D}_\varphi \Phi^k =: \mathbf{D}_k(\varphi) \quad (71)$$

$$\frac{\partial \mathbf{s}(k; \mathbf{u})}{\partial \mathbf{f}} = \mathbf{kB}\Phi^{k-1} =: \mathbf{D}_k(\mathbf{f})$$

The $\mathbf{I}_k(\mathbf{u})$ be defined as

$$\mathbf{I}_k(\mathbf{u}) = \frac{1}{\sigma^2} \text{Re} \begin{bmatrix} \mathbf{D}(\theta)^H \\ \mathbf{D}(\varphi)^H \\ \mathbf{D}(\mathbf{f})^H \end{bmatrix} \begin{bmatrix} \mathbf{D}(\theta)^H \\ \mathbf{D}(\varphi)^H \\ \mathbf{D}(\mathbf{f})^H \end{bmatrix}^H \quad (72)$$

So the Fisher information matrix is

$$\mathbf{I}(\mathbf{u}) = \sum_{k=1}^M \mathbf{I}_k(\mathbf{u}) = \frac{1}{\sigma^2} \text{Re} \begin{bmatrix} \Delta & \mathbf{P}^H & \mathbf{Q}^H \\ \mathbf{P} & \Lambda & \mathbf{R}^H \\ \mathbf{Q} & \mathbf{R} & \Gamma \end{bmatrix} \quad (73)$$

where M is the number of time samples, and

$$\Delta = \sum_{k=1}^M \Phi^{-k} \mathbf{D}_\theta^H \mathbf{D}_\theta \Phi^k \quad (74)$$

$$\Lambda = \sum_{k=1}^M \Phi^{-k} \mathbf{D}_\varphi^H \mathbf{D}_\varphi \Phi^k \quad (75)$$

$$\mathbf{\Gamma} = \sum_{k=1}^M k^2 \mathbf{\Phi}^{1-k} \mathbf{B}^H \mathbf{B} \mathbf{\Phi}^{k-1} \quad (76)$$

$$\mathbf{P} = \sum_{k=1}^M \mathbf{\Phi}^{-k} \mathbf{D}_{\varphi}^H \mathbf{D}_{\theta} \mathbf{\Phi}^k \quad (77)$$

$$\mathbf{Q} = \sum_{k=1}^M k \mathbf{\Phi}^{1-k} \mathbf{B}^H \mathbf{D}_{\theta} \mathbf{\Phi}^k \quad (78)$$

$$\mathbf{R} = \sum_{k=1}^M k \mathbf{\Phi}^{1-k} \mathbf{B}^H \mathbf{D}_{\varphi} \mathbf{\Phi}^k \quad (79)$$

5. SIMULATION RESULTS

Simulations experiments are conducted to evaluate the performance of the proposed method. In this section, the model of the cylindrical conformal antenna array is shown in Fig. 1(a). We assume that two far field, equal power signals s_1 and s_2 are impinging on the antenna array. The DOA and center frequency of s_1 are $\theta_1 = 60^\circ$, $\varphi_1 = 100^\circ$ and $f_1 = 1$ GHz, and those of s_2 are $\theta_1 = 50^\circ$, $\varphi_1 = 95^\circ$ and $f_2 = 2$ GHz, respectively. The data is sampled at a rate of 5 GHz, and the snapshot number is 200. The number of elements is 25, i.e., each sub-array has 8 elements. $k_{1\theta} = 0.5$, $k_{1\varphi} = 0.5$; $k_{2\theta} = 0.3$, $k_{2\varphi} = 0.7$, the element pattern is $g_{i\theta} = \sin(\theta'_j - \varphi'_j)$, $g_{i\varphi} = \cos(\theta'_j - \varphi'_j)$, θ'_j and φ'_j are the elevation and azimuth respectively for direction vector of the i th element in the local coordinate. The spatial rotation transformation of the element pattern from element local coordinates to array global coordinates could be found in [20]. All simulation results are based on 100 Monte Carlo simulation experiments (a computation method based on “random number”. The main idea is that the “frequency” of the events determines the “probability” of the events). A successful experiment is defined as the experiment with estimation error of less than 2 degree. The successful rate is defined as the proportion of the number of the successful experiments to the total number of the experiments.

An important part of frequency estimation is selecting the temporal smoothing parameter N . For frequency estimation, the primary computational cost concentrate on the eigendecomposition of a $4Nm \times 4Nm$ matrix, which has a complexity about $O(16N^2Lm^2) + O(64N^2Lm^2)$, meaning that the N should not be too large, because the computation cost could increase tremendously. Fig. 5 shows how temporal smoothing parameter N affects the frequency estimation

errors. From the curve, it is shown that the estimation performance of frequency gets better as parameter N increases. The extension of array manifold dimension is based on the time delay. The time aperture gets larger with the increasing temporal smoothing, which leads to higher estimation accuracy of frequency. The steering vector is a joint function of frequency and DOA. The estimation performance of DOA gets better as the estimation accuracy of frequency increases. In general condition, we should notice that the length of the observation time window is fixed, and the interval of sampling data depends on the sampling frequency of the system, so the total number of snapshot is deterministic. Increasing N too much will also result in the reduction of number of columns in the matrix \mathbf{X}_N (The number of the columns is $L - N + 1$). The sampling covariance matrix $\hat{\mathbf{R}}_{\mathbf{X}_N}$ is the asymptotic estimation of \mathbf{R} . The reduction of number of columns in \mathbf{X}_N will lead

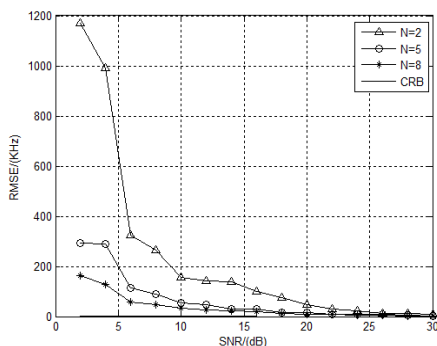


Figure 5. The frequency estimation error versus SNR.

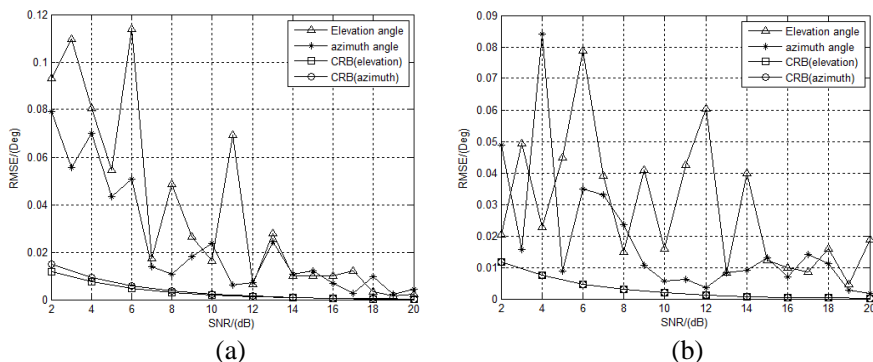


Figure 6. The DOA estimation error versus SNR. (a) DOA = (100°, 60°), (b) DOA = (95°, 55°).

to larger estimation error between the $\hat{\mathbf{R}}_{\mathbf{X}_N}$ and \mathbf{R} , which reduces the overall estimation accuracy of signal and noise subspace, so N should not be made too large in order to improve the system stability. The computation complexity of the proposed algorithm is related to L and N . So we must consider the trade-off between the computational complexity and estimation accuracy.

The effect of SNR (signal to noise ratio) on the DOA estimation error is shown in Fig. 6. In order to confirm the real-time processing ability of the proposed algorithm and reduce the effect of smoothing parameter on the performance of DOAs for two signals estimation, the smoothing parameter $N = 5$ is adopted in this paper. As shown in Figs. 6(a) and 6(b), DOAs are estimated accurately. When $\text{SNR} > 7$ dB, the root mean square error (RMSE) is almost less than 0.1 degree. The difference in estimation performance between azimuth angles and elevation angles has been caused by the different radiation patterns in these two directions. As the SNR increase, the DOA estimation error would approach the CRB for the proposed algorithm.

In Fig. 7(a), it is shown that, apart from the estimation error, the success rate is also improved by increasing SNR. When $\text{SNR} > 5$ dB, the success rate would reach 100% in the condition that the snapshot number is 200 (In the simulation experiment, the snapshot is that all the elements of the array sample the data at the same time for just one time. the snapshot number is the number of the sampling snapshot which is used for simulation.). It is shown in Fig. 7(b) that when $\text{SNR} > 0$ dB, the success rate would reach 100% in the condition that the snapshot number is 1000. Thus increasing the snapshot number could improve the success rate just as increasing SNR.

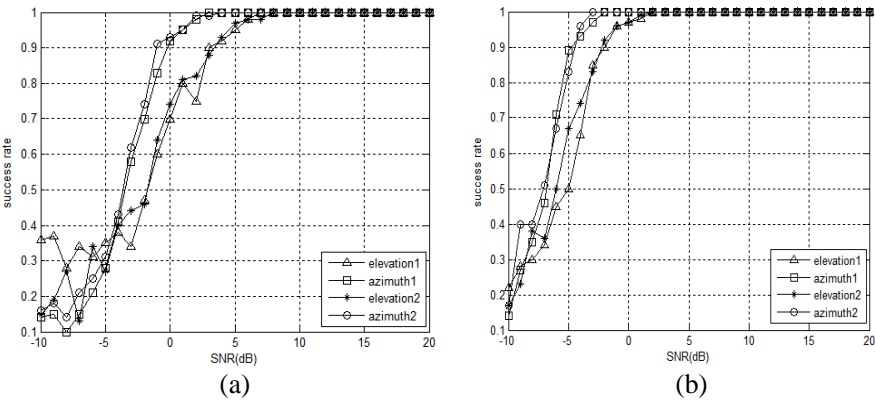


Figure 7. (a) The success rate versus SNR at snapshot number 200. (b) The success rate versus SNR at snapshot number 1000.

6. CONCLUSIONS

In this paper, a novel integrated frequency and DOA estimation method is proposed for cylindrical conformal antenna array. The pattern of each element in conformal array has a different direction because of the varying curvature of conformal carrier, which makes most modeling or parameter estimation techniques used for planar array unsuitable in this condition. Three key techniques are developed in this paper. Firstly, the frequencies estimation of signal sources is obtained by constructing state-space matrix. Secondly, the decoupling method for DOA and polarization parameters is implemented via PM algorithm. Thirdly, the interpolation technique is utilized to complete the pairing between frequencies and DOAs. Based on the above techniques, the parameters of combined frequency and DOA estimation could be computed efficiently and accurately. The pairing approach based on interpolation technique could be used for any arbitrary conformal arrays. Numerical results indicate that the proposed algorithm is effective and accurate for the combined frequency and DOA estimation on cylindrical conformal antenna array.

ACKNOWLEDGMENT

The authors would like to thank the editor and anonymous reviewers for their valuable comments and suggestion. In addition, this work was supported in part by the National Natural Science Foundation of China under Grant 61201410 and in part by Fundamental Research Focused on Special Fund Project of the Central Universities (Program No. HEUCFZ1215).

REFERENCES

1. Josefsson, L. and P. Persson, *Conformal Array Antenna Theory and Design*, IEEE Press Series on Electromagnetic Wave Theory, 2006.
2. Balanis, C. A., *Antenna Theory: Analysis and Design*, Wiley, New York, 2005.
3. Wang, J. J. and Y. P. Zhang, "Circuit model of microstrip patch antenna on ceramic land grid array package for antenna-chip codesign of highly integrated RF transceivers," *Progress In Electromagnetics Research*, Vol. 117, 83–101, 2011.
4. Asimakis, N. P., I. S. Karanasiou, and N. K. Uzunoglu, "Non-invasive microwave radiometric system for intracranial

- applications: A study using the conformal L-notch microstrip patch antenna,” *Progress In Electromagnetics Research*, Vol. 117, 83–101, 2011.
5. Wang, X., M. Zhang, and S. J. Wang, “Practicability analysis and application of PBG structures on cylindrical conformal microstrip antenna and array,” *Progress In Electromagnetics Research*, Vol. 115, 495–507, 2011.
 6. Kong, L. Y., J. Wang, and W. Y. Yin, “A novel dielectric conformal FDTD method for computing SAR distribution of the human body in a metallic cabin illuminated by an intentional electromagnetic pulse (IEMP),” *Progress In Electromagnetics Research*, Vol. 126, 355–373, 2012.
 7. Boeringer, D. W., D. H. Werner, and D. W. Machuga, “A simultaneous parameter adaptation scheme for genetic algorithms with application to phased array synthesis,” *IEEE Trans. on Antennas and Propag.*, Vol. 53, No. 1, 356–371, 2005.
 8. Vaskelainen, L. I., “Constrained least-squares optimization in conformal array antenna synthesis,” *IEEE Trans. on Antennas and Propag.*, Vol. 55, No. 3, 859–867, 2007.
 9. Li, W. T., Y. Q. Hei, and X. W. Shi, “Pattern synthesis of conformal arrays by a modified particle swarm optimization,” *Progress In Electromagnetics Research*, Vol. 117, 237–252, 2011.
 10. Xu, Z., H. Li, and Q. Z. Liu, “Pattern synthesis of conformal antenna array by the hybrid genetic algorithm,” *Progress In Electromagnetics Research*, Vol. 79, 75–90, 2008.
 11. Liang, J. and D. Liu, “Two L-shaped array-based 2-D DOAs estimation in the presence of mutual coupling,” *Progress In Electromagnetics Research*, Vol. 112, 273–298, 2011.
 12. Zhang, Y., Q. Wan, and A.-M. Huang, “Localization of narrow band sources in the presence of mutual coupling via sparse solution finding,” *Progress In Electromagnetics Research*, Vol. 86, 243–257, 2008.
 13. Pouramadi, M., M. Nakhkash, and A. A. Tadion, “Application of MDL criterion for microwave imaging by music algorithm,” *Progress In Electromagnetics Research B*, Vol. 40, 261–278, 2012.
 14. Gu, X. and Y. Zhang, “Resolution threshold analysis of MUSIC algorithm in radar range imaging,” *Progress In Electromagnetics Research B*, Vol. 31, 297–321, 2011.
 15. Yang, P., F. Yang, and Z. P. Nie, “DOA estimation with sub-array divided technique and interpolated esprit algorithm on a cylindrical conformal antenna array,” *Progress In*

- Electromagnetics Research*, Vol. 103, 201–216, 2010.
16. Yang, P., F. Yang, and Z. P. Nie, “DOA estimation using MUSIC algorithm on a cylindrical conformal antenna array,” *IEEE Antennas and Propagation Symposium*, 5299–5302, 2007.
 17. Solimene, R., A. Dell’Aversano, and G. Leone, “Interferometric time reversal music for small scatterer localization,” *Progress In Electromagnetics Research*, Vol. 131, 243–258, 2012.
 18. Lee, J. H., Y. S. Jeong, S. W. Cho, W. Y. Yeo, and K. S. J. Pister, “Application of the Newton method to improve the accuracy of TOA estimation with the beamforming algorithm and the MUSIC algorithm,” *Progress In Electromagnetics Research*, Vol. 116, 243–258, 2011.
 19. Bencheikh, M. L. and Y. Wang, “Combined ESPRIT-RootMUSIC for DOA-DOD estimation in polarimetric bistatic MIMO radar,” *Progress In Electromagnetics Research Letters*, Vol. 22, 109–117, 2011.
 20. Wang, B. H., Y. Guo, Y. L. Wang, and Y. Z. Lin, “Frequency-invariant pattern synthesis of conformal array antenna with low cross-polarisation,” *IET Microw. Antennas Propag.*, Vol. 2, No. 5, 442–450, 2008.
 21. Li, F. and R. J. Vaccaro, “On frequency-wavenumber estimation by state-space realization,” *IEEE Trans. Circuits and Systems*, Vol. 38, No. 7, 800–804, 1991.
 22. Lemma, A. N., A. J. Veen, and E. F. Deprettere, “Analysis of joint angle-frequency estimation using ESPRIT,” *IEEE Trans. Signal Processing*, Vol. 51, No. 5, 1264–1283, 2003.
 23. Sanchez-Araujo, J. and S. Marcos, “Statistical analysis of the propagator method for estimation without eigendecomposition,” *Statistical Signal and Array Process.*, Vol. 10, No. 8, 570–573, 1996.
 24. Weiss, A. J. and M. Gavish, “Direction finding using ESPRIT with interpolated arrays,” *IEEE Trans. Signal Processing*, Vol. 39, No. 6, 1473–1478, 1991.
 25. Friedlander, B. and A. J. Weiss, “Direction finding for wide-band signals using an interpolated array,” *IEEE Trans. Signal Processing*, Vol. 41, No. 4, 1618–1634, 1993.
 26. Yuen, N. and B. Friedlander, “Asymptotic performance analysis of ESPRIT, higher order ESPRIT, and virtual ESPRIT algorithms,” *IEEE Trans. Signal Processing*, Vol. 44, No. 10, 2537–2550, 1996.
 27. Kay, S. M., *Fundamentals of Statistical Signal Processing: Estimation Theory*, Prentice-Hall, Englewood Cliffs, NJ, 1993.